ChemComm

COMMUNICATION

View Article Online
View Journal | View Issue

Cite this: *Chem. Commun.*, 2022, **58**, 9548

Received 6th June 2022,
Accepted 25th July 2022

DOI: 10.1039/d2cc03179e

rsc.li/chemcomm

A hybrid ZIF-8/ZIF-62 glass membrane for gas separation†

Yating Zhang,[a] Yichen Wang,[a] Huanni Xia,[a] Peng Gao,[b] Yi Cao,*[ac] Hua Jin *[a] and Yanshuo Li *[ac]

Metal–organic framework (MOF) glasses have demonstrated great potential for high-performance separation. Herein a uniform hybrid MOF glass membrane was fabricated by using the liquid state of ZIF-62 to facilitate the melting of ZIF-8. The doping of ZIF-8 enhanced both the adsorption capacity as well as the ideal C_3H_6/C_3H_8 selectivity of ZIF-62 glass. As expected, the hybrid glass membrane exhibited good C_3H_6/C_3H_8 separation performance while preserving the CO_2 performance of the sole ZIF-62 membrane.

Metal–organic frameworks (MOFs) represent one of the most impressive kinds of membrane materials because of their high porosity and tunable chemistry.[1,2] The development of MOF-based membranes has been very prosperous over the past dozen years.[3–5] To achieve membranes with excellent performance, many challenges such as the unavoidable grain-boundary defects in the polycrystalline membranes and poor MOF-polymer interface compatibility in the mixed matrix membranes[6] must be addressed. Very recently, a new state of MOF material named MOF glasses (a_gMOF),[7–10] which could be fabricated by melting and then quenching some crystalline MOFs, have attracted much attention due to their non-crystalline structures, intrinsic porosity, and easy processibility.[11–14] The fascinating properties endow MOF glasses with great potential in solving the above-mentioned challenges in MOF-based membranes.

Wang *et al.*[15] reported a ZIF-62 glass membrane for carbon capture. The polycrystalline ZIF-62 membrane *via in situ* solvothermal synthesis had significant gaps, pinholes, and grain boundary features. After melt-quenching treatment, the achieved glass membrane exhibited a very smooth surface without grain boundaries. Thus, in contrast to the leaking polycrystalline membrane, the glass membrane exhibited high separation performance for CO_2/N_2 and CO_2/CH_4 mixtures with separation factors of 34 and 36. Lin *et al.*[16] fabricated a 6FDA-DAM polyimide-based composite membrane with ZIF-62 as filler. It was confirmed that the *in situ* melting of ZIF-62 within the polyimide matrix was very effective in reducing meso- and macroscale defects at the MOF/polymer interface, resulting in a 23.7% increase in CO_2/N_2 selectivity. Except for the a_gZIF-62 and $a_g(\text{ZIF-62})_{0.2}(\text{6FDA-DAM})_{0.8}$ membrane, other MOF glass membranes such as M-P-dmbIm[17] and TIF-4 membranes[18] also showed outstanding CO_2 separation performance.

Unlike more than 60 000 MOF structures in the Cambridge Structural Database, the number of reported disordered MOF liquid and glass is very limited.[19] Thus, it might be difficult to find the suitable glass material for target mixture separation through extensive screening. Under such a background, the construction of MOF glass-based hybrid materials could be a good solution. A flux melted glass sample $a_g[(\text{ZIF-8})_{0.2}(\text{ZIF-62})_{0.8}]$ was fabricated by the flux melting of the crystalline ZIF-8 *via* the high-temperature ZIF-62 liquid.[20] Hou *et al.*[21] constructed the MOF crystal-glass composites *via* dispersing crystalline MIL-53 within the ZIF-62-glass matrix. Despite the several reports about MOF glass-based hybrid materials,[22–24] their application in membrane separation remains undeveloped.

Herein we report a hybrid ZIF-8/ZIF-62 glass membrane by using the liquid state of ZIF-62 to facilitate the melting of ZIF-8. As compared to the pure ZIF-62 glass membrane, the resultant hybrid glass membrane demonstrates the ability for propylene (C_3H_6) and propane (C_3H_8) separation.

First, we prepared a series of hybrid ZIF-8/ZIF-62 glass materials with different doping amounts of ZIF-8 and then investigated their adsorption properties toward C3 hydrocarbons. ZIF-8 and ZIF-62 crystals (Fig. S1, ESI†) in a certain mass proportion were mixed well *via* the mechanical ball-milling process, and the obtained mixtures were named $(\text{ZIF-8})_x(\text{ZIF-62})_{1-x}$. As shown from their powder X-ray diffraction (XRD) pattern (Fig. S2, ESI†), the intensity of the Bragg peaks of ZIF-8 divided by that of ZIF-62 gradually enhanced with the increased content of ZIF-8 as expected. The thermal behavior of the

[a] *School of Material Science and Chemical Engineering, Ningbo University, Ningbo 315211, China. E-mail: caoyi@nbu.edu.cn, jinhua@nbu.edu.cn*
[b] *Ningbo Kingfa Advanced Materials Co., Ltd, Ningbo, 315000, China*
[c] *Hymater Co. Ltd., 777 Qingfeng Road, Ningbo 315000, China. E-mail: liyanshuo@nbu.edu.cn*

† Electronic supplementary information (ESI) available: Experimental details and addition figures and tables. See DOI: https://doi.org/10.1039/d2cc03179e

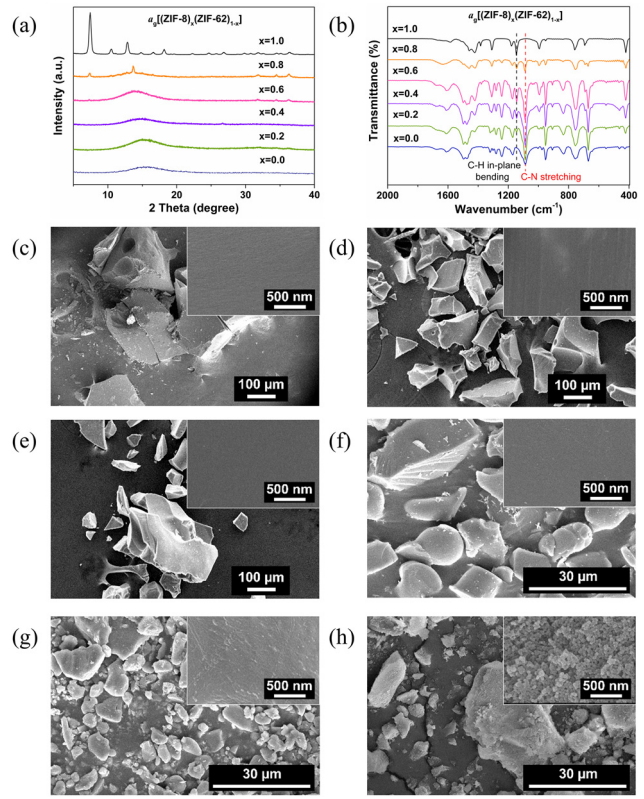

Fig. 1 (a) PXRD patterns and (b) FTIR spectra of $a_g[(ZIF\text{-}8)_x(ZIF\text{-}62)_{1-x}]$. SEM images of $a_g[(ZIF\text{-}8)_x(ZIF\text{-}62)_{1-x}]$ with x of (c) 0, (d) 0.2, (e) 0.4, (f) 0.6, (g) 0.8 and (h) 1, respectively.

mixtures was evaluated with thermal gravimetry (TG) and differential scanning calorimetry (DSC) measurements (Fig. S3, ESI†). It was found that the doping of ZIF-8 had little effect on the melting temperature of ZIF-62 around 430 °C. Then, the $(ZIF\text{-}8)_x(ZIF\text{-}62)_{1-x}$ crystal mixtures were employed for fabricating glass-based composites by the melt-quenching process at 500 °C since all samples could remain stable up to 500 °C. Most of the resultant $a_g[(ZIF\text{-}8)_x(ZIF\text{-}62)_{1-x}]$ samples except the one with x of 0.8 didn't exhibit Bragg diffraction, suggesting the glassy nature (Fig. 1a). Some diffraction peaks of ZIF-8 were still retained for $a_g[(ZIF\text{-}8)_{0.8}(ZIF\text{-}62)_{0.2}]$ sample, which might be due to the absence of enough liquid ZIF-62 for promoting the flux melting of ZIF-8. As shown from the FTIR spectra (Fig. 1b and Fig. S4, ESI†), the mixture powders retained their chemical bond connection regardless of the mechanical ball milling or the vitrification process. The morphologies of $a_g[(ZIF\text{-}8)_x(ZIF\text{-}62)_{1-x}]$ samples were then measured, and the results were given in Fig. 1c–h. The pure a_gZIF-62 presents a smooth surface. When the ZIF-8 doping content was within the range of 20–60%, the liquid state of ZIF-62 succeeded in facilitating the melting of ZIF-8, as indicated by their smooth and dense surface. In contrast, when the ZIF-8 content was as high as 80%, some particles were embedded in the glass melt. This result was consistent with the XRD patterns, indicating that ZIF-8 was not completely melted under this condition.

The adsorption property of all hybrid glass samples toward C_3H_6 and C_3H_8 was investigated (Fig. 2a and Fig. S5, ESI†). With the increase of ZIF-8 content, the adsorption capacity of hybrid glass $a_g[(ZIF\text{-}8)_x(ZIF\text{-}62)_{1-x}]$ for both C_3H_6 and C_3H_8 gradually increased. On the other hand, amorphous ZIF-8 performs far well in the separation of C_3H_6/C_3H_8 than crystal ZIF-8. As a result, $a_g[(ZIF\text{-}8)_x(ZIF\text{-}62)_{1-x}]$ samples (within the range of x = 0.2–0.6), amorphous as proved by the XRD results, had notably better selectivity than $a_g[(ZIF\text{-}8)_{0.8}(ZIF\text{-}62)_{0.2}]$ and a_gZIF-62 (Fig. 2b). In summary, it is believed that the doping of ZIF-8 enhanced both the adsorption capacity as well as the ideal selectivity of C_3H_6 and C_3H_8.

The hybrid ZIF-8/ZIF-62 glass membrane was then fabricated *via* melt-quenching of the corresponding polycrystalline membrane. First, the post-synthetic ligand exchange approach was employed for preparing the mixed-phase polycrystalline membrane. A prepared ZIF-62 membrane was immersed in the DMF solution containing 2-methylimidazole ligand of ZIF-8 to react at 50 °C for 2 h. The XRD pattern (Fig. S6, ESI†) revealed that ZIF-62 partially converted into ZIF-8, forming a ZIF-62/ZIF-8 mixed-phase membrane. SEM images showed that the surface of the obtained hybrid membrane mostly presented the crystal morphology of ZIF-8 (Fig. S7, ESI†). After heat treatment, an amorphous membrane without any diffraction characteristic peaks could be obtained. However, the membrane was not continuous or dense, deviating from the smooth surface properties of glass. It could be attributed to the fact that the melting of ZIF-8/ZIF-62 performed well only when the two phases were tightly combined. The particles due to the incomplete melting made this method not feasible.

Further, we successfully prepared the polycrystalline ZIF-8/ZIF-62 hybrid membrane by the *in situ* solvothermal reaction (Fig. 3a and Fig. S8, ESI†). SEM images showed that the surface of the membrane had particles with obvious crystal shapes (Fig. 3c). After melting- quenching process, the particles on the surface disappeared completely (Fig. 3d). Similar to the melting behavior of the ZIF-62 glass, the molten liquid phase would penetrate the nanopores of the alumina support through capillary force, enhancing the mechanical strength and stability of the membrane (Fig. 3b). A single-ligand control experiment was also conducted. It was found that the reaction of a single ZIF-8 or ZIF-62 organic ligand could only lead to amorphous substances rather than polycrystalline membranes (Fig. S9–S11, ESI†). For the as-obtained membranes after heat treatment, this

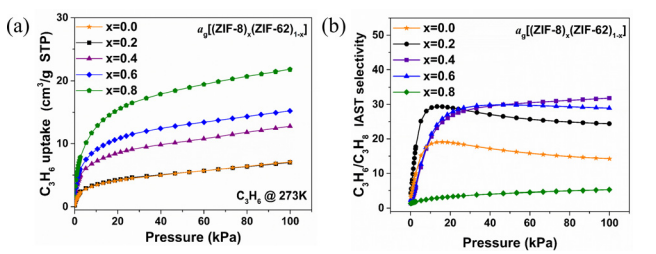

Fig. 2 (a) C_3H_6 adsorption isotherms and (b) C_3H_6/C_3H_8 IAST selectivities of $a_g[(ZIF\text{-}8)_x(ZIF\text{-}62)_{1-x}]$ at 273 K.

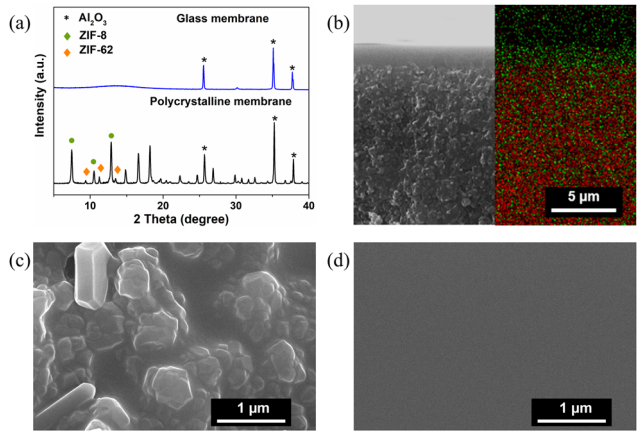

Fig. 3 (a) XRD patterns of ZIF-8/ZIF-62 polycrystalline membrane and glass membranes. (b) EDXS-mapping of glass membrane, including the membrane on the surface and the infiltration part in the top layer of the alumina support; green Zn and red Al. Top SEM images of (c) ZIF-8/ZIF-62 polycrystalline membrane and (d) glass membrane.

amorphous substance disappeared and no gas separation performance was noted. This shows that the corresponding hybrid glass membrane was the result of the synergistic effects of ZIF-8/ZIF-62. The obtained hybrid ZIF-8/ZIF-62 glass possessed the ZIF-8 mass ratio of 63 wt% as calculated by the ^{1}H NMR spectra (Fig. S12, ESI†), which was suitable for C_3H_6/C_3H_8 separation as indicated by the adsorption results of hybrid glasses.

Gas permeation property of the resultant hybrid membranes was evaluated using the Wicke–Kallenbach method. The single gas permeance as a function of the molecular kinetic diameter was shown in Fig. 4a. Compared with the ZIF-62 glass membrane, the hybrid ZIF-8/ZIF-62 glass membrane had two obvious cut-offs between CO_2/N_2 and C_3H_6/C_3H_8. As shown in Fig. 4b, the ideal selectivity values of all gas pairs were higher than the Knudsen selectivity values, identifying the excellent

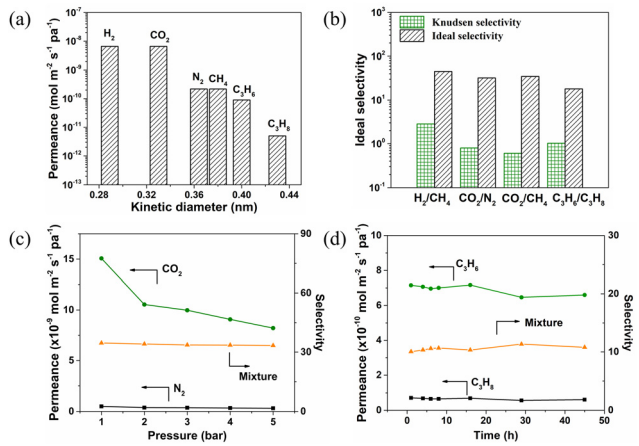

Fig. 4 (a) Single gas permeance as a function of the gas kinetic diameter, and (b) the corresponding ideal selectivities. (c) Pressure dependence of the hybrid glass membrane for CO_2/N_2 separation at 25 °C with 1 : 1 CO_2/N_2 feed. (d) Long-term stability of the hybrid glass membrane for C_3H_6/C_3H_8 separation.

molecular sieve performance of the hybrid membrane. The selectivity values of small molecular gases, *i.e.*, H_2/CH_4 (45), CO_2/N_2 (32), and CO_2/CH_4 (35), were similar to our previously reported a_gZIF-62 membrane.[15] However, it should be noted that the ideal selectivity of the C_3H_6/C_3H_8 gas pair reached 17, significantly higher than the a_gZIF-62 membrane (2.5). ZIF-8 in the hybrid glass has indeed play an important role which might be ascribed to the following two reasons, (1) the formed amorphous ZIF-8 after melting is highly selective for C_3H_6,[25] (2) the doping of ZIF-8 increases the pore limiting aperture of a_gZIF-62.[20] These differences might explain the potential of the hybrid glass membrane for propylene/propane separation.

The hybrid glass membranes were also tested with binary gas mixtures. The selectivities for equimolar CO_2/N_2 and CO_2/CH_4 mixture were 34.6 (Fig. 4c) and 29.9 (Table S1, ESI†), respectively, preserving the separation characteristics of the ZIF-62 membrane for small molecule gases. On the other hand, the separation selectivity for C_3H_6/C_3H_8 could reach 18.7 (Table S1, ESI†), achieving a breakthrough in the a_gZIF-62 membrane for larger molecule gas. The permeance and separation factor as a function of pressure was also studied (Fig. 4c). Although the permeability of CO_2 and N_2 both gradually decreased with the increase of pressure, the separation factor of CO_2/N_2 was almost unchanged. It indicates that the doping of ZIF-8 enhanced the pressure resistance of the a_gZIF-62 glass membrane. A 45 h test on CO_2/N_2 (Fig. S13, ESI†) and C_3H_6/C_3H_8 (Fig. 4d) separation was also carried out, respectively. The performance had very little, if any, declination, showing relatively long-term stability.

In summary, this study verifies the benefits of the creative addition of MOF crystals to MOF glass. ZIF-8 can be effectively melted under the flux of ZIF-62 to form a flux melted glass membrane. While preserving the separation performance of the ZIF-62 glass membrane for small molecule gases, the hybrid glass membrane also showed enhanced separation ability for macromolecular gases (olefins/alkanes). Moreover, the hybrid glass membrane has an excellent 45 h stability, which is conducive to its potential for practical applications. We are also trying hard to explore the separation mechanism of MOF glass-based hybrid membranes and thus make a wider application scope for MOF glasses.

This work was financially supported by the National Natural Science Foundation of China (No. 22178182 and 22178183), Zhejiang Provincial Natural Science Foundation of China (No. LY21B060002), Ningbo Natural Science Foundation (No. 2021J081), The Fund of Science and Technology on Surface Physics and Chemistry Laboratory (No. XKFZ202003).

Conflicts of interest

There are no conflicts to declare.

Notes and references

1 Q. Qian, P. A. Asinger, M. J. Lee, G. Han, K. Mizrahi Rodriguez, S. Lin, F. M. Benedetti, A. X. Wu, W. S. Chi and Z. P. Smith, *Chem. Rev.*, 2020, **120**, 8161–8266.

2 S. Qiu, M. Xue and G. Zhu, *Chem. Soc. Rev.*, 2014, **43**, 6116–6140.
3 Q. Hou, S. Zhou, Y. Wei, J. Caro and H. Wang, *J. Am. Chem. Soc.*, 2020, **142**, 9582–9586.
4 Q. Ma, K. Mo, S. Gao, Y. Xie, J. Wang, H. Jin, A. Feldhoff, S. Xu, J. Y. S. Lin and Y. Li, *Angew. Chem., Int. Ed.*, 2020, **59**, 21909–21914.
5 C. Wang, Y. Sun, L. Li, R. Krishna, T. Ji, S. Chen, J. Yan and Y. Liu, *Angew. Chem., Int. Ed.*, 2022, e202203663.
6 Y. Zhang, X. Feng, S. Yuan, J. Zhou and B. Wang, *Inorg. Chem. Front.*, 2016, **3**, 896–909.
7 T. D. Bennett, Y. Yue, P. Li, A. Qiao, H. Tao, N. G. Greaves, T. Richards, G. I. Lampronti, S. A. Redfern, F. Blanc, O. K. Farha, J. T. Hupp, A. K. Cheetham and D. A. Keen, *J. Am. Chem. Soc.*, 2016, **138**, 3484–3492.
8 A. W. Thornton, K. E. Jelfs, K. Konstas, C. M. Doherty, A. J. Hill, A. K. Cheetham and T. D. Bennett, *Chem. Commun.*, 2016, **52**, 3750–3753.
9 S. Horike, S. S. Nagarkar, T. Ogawa and S. Kitagawa, *Angew. Chem., Int. Ed.*, 2020, **59**, 6652–6664.
10 R. S. K. Madsen, A. Qiao, J. Sen, I. Hung, K. Chen, Z. Gan, S. Sen and Y. Yue, *Science*, 2020, **367**, 1473–1476.
11 T. D. Bennett and A. K. Cheetham, *Acc Chem. Res.*, 2014, **47**, 1555–1562.
12 C. Zhou, L. Longley, A. Krajnc, G. J. Smales, A. Qiao, I. Erucar, C. M. Doherty, A. W. Thornton, A. J. Hill, C. W. Ashling, O. T. Qazvini, S. J. Lee, P. A. Chater, N. J. Terrill, A. J. Smith, Y. Yue, G. Mali, D. A. Keen, S. G. Telfer and T. D. Bennett, *Nat. Commun.*, 2018, **9**, 5042.
13 S. Li, R. Limbach, L. Longley, A. A. Shirzadi, J. C. Walmsley, D. N. Johnstone, P. A. Midgley, L. Wondraczek and T. D. Bennett, *J. Am. Chem. Soc.*, 2019, **141**, 1027–1034.
14 M. Stepniewska, M. B. Østergaard, C. Zhou and Y. Yue, *J. Non-Cryst. Solids*, 2020, **530**, 119806.
15 Y. Wang, H. Jin, Q. Ma, K. Mo, H. Mao, A. Feldhoff, X. Cao, Y. Li, F. Pan and Z. Jiang, *Angew. Chem., Int. Ed.*, 2020, **59**, 4365–4369.
16 R. Lin, J. Hou, M. Li, Z. Wang, L. Ge, S. Li, S. Smart, Z. Zhu, T. D. Bennett and V. Chen, *Chem. Commun.*, 2020, **56**, 3609–3612.
17 J. Li, J. Wang, Q. Li, M. Zhang, J. Li, C. Sun, S. Yuan, X. Feng and B. Wang, *Angew. Chem., Int. Ed.*, 2021, **39**, 21474–21479.
18 H. Xia, H. Jin, Y. Zhang, H. Song, J. Hu, Y. Huang and Y. Li, *J. Membr. Sci.*, 2022, **655**, 120611.
19 T. D. Bennett and S. Horike, *Nat. Rev. Mater.*, 2018, **3**, 431–440.
20 L. Longley, S. M. Collins, S. Li, G. J. Smales, I. Erucar, A. Qiao, J. Hou, C. M. Doherty, A. W. Thornton, A. J. Hill, X. Yu, N. J. Terrill, A. J. Smith, S. M. Cohen, P. A. Midgley, D. A. Keen, S. G. Telfer and T. D. Bennett, *Chem. Sci.*, 2019, **10**, 3592–3601.
21 J. Hou, C. W. Ashling, S. M. Collins, A. Krajnc, C. Zhou, L. Longley, D. N. Johnstone, P. A. Chater, S. Li, M. V. Coulet, P. L. Llewellyn, F. X. Coudert, D. A. Keen, P. A. Midgley, G. Mali, V. Chen and T. D. Bennett, *Nat. Commun.*, 2019, **10**, 2580.
22 L. Longley, S. M. Collins, C. Zhou, G. J. Smales, S. E. Norman, N. J. Brownbill, C. W. Ashling, P. A. Chater, R. Tovey, C. B. Schonlieb, T. F. Headen, N. J. Terrill, Y. Yue, A. J. Smith, F. Blanc, D. A. Keen, P. A. Midgley and T. D. Bennett, *Nat. Commun.*, 2018, **9**, 2135.
23 Z. Zhang, A. Simon, C. Abetz, M. Held, A. L. Hohme, E. S. Schneider, T. Segal-Peretz and V. Abetz, *Adv. Mater.*, 2021, **33**, e2105251.
24 J. Hou, P. Chen, A. Shukla, A. Krajnc, T. Wang, X. Li, R. Doasa, L. H. G. Tizei, B. Chan, D. N. Johnstone, R. Lin, T. U. Schülli, I. Martens, D. Appadoo, M. S. Ari, Z. Wang, T. Wei, S.-C. Lo, M. Lu, S. Li, E. B. Namdas, G. Mali, A. K. Cheetham, S. M. Collins, V. Chen, L. Wang and T. D. Bennett, *Science*, 2021, **374**, 621–625.
25 Q. Ma, H. Jin and Y. Li, *Chem. – Eur. J.*, 2020, **26**, 13137–13141.